Study of $e^+e^- \to \omega\pi^0 \to \pi^0\pi^0\gamma$ in the energy range 1.05–2.00 GeV with the SND detector

M. N. Achasov,[1,2] V. M. Aulchenko,[1] A. Yu. Barnyakov,[1] K. I. Beloborodov,[1,2] A. V. Berdyugin,[1,2] A. G. Bogdanchikov,[1]
A. A. Botov,[1] T. V. Dimova,[1] V. P. Druzhinin,[1,2] V. B. Golubev,[1,2] K. A. Grevtsov,[1,2] L. V. Kardapoltsev,[1,2,*]
A. G. Kharlamov,[1,2] D. P. Kovrizhin,[1] I. A. Koop,[1,2] A. A. Korol,[1,2] S. V. Koshuba,[1] A. P. Lysenko,[1] K. A. Martin,[1,3]
I. N. Nesterenko,[1] A. E. Obrazovsky,[1] E. V. Pakhtusova,[1] E. A. Perevedentsev,[1,2] A. L. Romanov,[1,2] S. I. Serednyakov,[1,2]
Z. K. Silagadze,[1,2] K. Yu. Skovpen,[1] A. N. Skrinsky,[1] I. K. Surin,[1] Yu. A. Tikhonov,[1,2] A. V. Vasiljev,[1] P. Yu. Shatunov,[1]
Yu. M. Shatunov,[1] D. A. Shtol,[1] A. L. Romanov,[1,2] and I. M. Zemlyansky[1]

[1]*Budker Institute of Nuclear Physics, SB RAS, Novosibirsk 630090, Russia*
[2]*Novosibirsk State University, Novosibirsk 630090, Russia*
[3]*Novosibirsk State Technical University, Novosibirsk 630092, Russia*

The cross section for the process $e^+e^- \to \omega\pi^0 \to \pi^0\pi^0\gamma$ has been measured in the center-of-mass energy range 1.05–2.00 GeV. The experiment has been performed at the e^+e^- collider VEPP-2000 with the SND detector. The measured $e^+e^- \to \omega\pi^0$ cross section above 1.4 GeV is the most accurate to date. Below 1.4 GeV our data are in good agreement with the previous SND and CMD-2 measurements. Data on the $e^+e^- \to \omega\pi^0$ cross section are well described by the vector meson dominance model with two excited ρ-like states. From the measured cross section we have extracted the $\gamma^* \to \omega\pi^0$ transition form factor. It has been found that the vector meson dominance model cannot describe simultaneously our data and data obtained from the $\omega \to \pi^0\mu^+\mu^-$ decay. We have also tested the conserved vector current hypothesis comparing our results on the $e^+e^- \to \omega\pi^0$ cross section with data on the $\tau^- \to \omega\pi^-\nu_\tau$ decay and have found that the conserved vector current hypothesis works well within the reached experimental accuracy of about 5%.

I. INTRODUCTION

Experiments with the SND detector [1] at the e^+e^- collider VEPP-2000 [2] started in 2010. The main goals of these experiments are a high precision measurement of the total cross section of $e^+e^- \to$ hadrons in the center-of-mass (c.m.) energy range up to 2 GeV and the investigation of the vector meson excitations with masses between 1 and 2 GeV/c^2. In this connection, a study of the process

$$e^+e^- \to \omega\pi^0 \to \pi^0\pi^0\gamma \qquad (1)$$

is very topical. The process $e^+e^- \to \omega\pi^0$ is one of the dominant hadronic processes contributing to the total hadronic cross section at the c.m. energy between 1 and 2 GeV. As one of the important decay modes of the isovector vector states $\rho(1450)$ and $\rho(1700)$, it can provide a lot of information about their properties. Moreover, this measurement can be used to check the relation between the $e^+e^- \to \omega\pi^0$ cross section and the differential rate in the $\tau^- \to \omega\pi^-\nu_\tau$ decay following from the conservation of vector current and isospin symmetry [conserved vector current (CVC) hypothesis] [3]. The SND plans to search for electric dipole decays of the $\rho(1450)$ and $\rho(1700)$ mesons to the $\pi^0\pi^0\gamma$ final state, which are important for an understanding of the $\rho(1450)$ and $\rho(1700)$ quark structure. The process $e^+e^- \to \omega\pi^0$ is the main background for this search;

its precise measurement is the first step in investigating the $\rho(1450)$ and $\rho(1700)$ radiative decays.

In this work the process $e^+e^- \to \omega\pi^0$ is studied in the ω decay mode to $\pi^0\gamma$. Despite the fact that the main ω decay mode to $\pi^+\pi^-\pi^0$ has a probability about an order of magnitude higher, this choice looks reasonable. Unlike the 4π final state, the $\omega\pi^0$ intermediate mechanism is dominant in the $\pi^0\pi^0\gamma$ final state in the energy range under study. This makes it possible to avoid systematic uncertainties due to both the complex procedure of subtracting background and taking into account interference between different intermediate mechanisms.

The process $e^+e^- \to \omega\pi^0$ in the $\omega \to \pi^0\gamma$ decay mode was first studied in the ND experiment [4] at the VEPP-2M collider. The cross section was measured at c.m. energies below 1.4 GeV. Later this measurement was repeated by the SND [5] and CMD-2 [6] detectors with much higher statistics. In the energy region near the ϕ-meson resonance, the cross section was measured in the SND experiment [7] and then in the KLOE experiment [8]. Our measurement of the $e^+e^- \to \omega\pi^0 \to \pi^0\pi^0\gamma$ cross section at VEPP-2000 based on 5 pb^{-1} collected in 2010 was published in Ref. [9].

The first measurement of the process $e^+e^- \to \omega\pi^0$ in the $\omega \to \pi^+\pi^-\pi^0$ decay mode was performed by the DM2 Collaboration [10]. For a long time this measurement was the only one above 1.4 GeV. Below 1.4 GeV this cross section was measured at VEPP-2M by SND [7,11] and CMD-2 [12], and in the KLOE experiment [8] in the ϕ-meson region.

*l.v.kardapoltsev@inp.nsk.su

II. EXPERIMENT

SND [1] is a general purpose nonmagnetic detector. Its main part is a spherical three-layer NaI(Tl) calorimeter with 560 individual crystals per layer and 90% solid angle coverage. The calorimeter energy resolution for photons is $\sigma_E/E_\gamma = 4.2\%/\sqrt[4]{E_\gamma \text{ (GeV)}}$, the angular resolution $\simeq 1.5°$. There is a tracking system around the collider beam pipe based on a nine-layer drift chamber and a one-layer proportional chamber with cathode-strip read-out. Outside the calorimeter a muon detector consisting of proportional tubes and scintillation counters is placed. An aerogel Cherenkov counter located between the drift chamber and the calorimeter is used for particle identification.

Experiments at VEPP-2000 started in 2010. During 2010–2012 the c.m. energy range $E = 1.05$–2.00 GeV was scanned several times with a step of 20–25 MeV. The total integrated luminosity collected by SND in this energy range is about 40 pb^{-1}. This work is based on data (27 pb^{-1}) recorded in 2010–2011.

During the experiment, beam energy was determined using measurements of the magnetic field in the collider bending magnets. To fix the absolute energy scale, a scan of the $\phi(1020)$ resonance was performed and its mass was measured. However, possible instability and uncertainties in collider components may lead to a sizable energy bias when the beam energy increases from 0.5 to 1 GeV. The uncertainty in the energy setting was investigated in 2012 in special runs, in which the beam energy was measured using the Compton backscattering method [13]. Based on the results of these runs we conservatively estimate the uncertainty in the c.m. energy to be 5 MeV.

III. LUMINOSITY MEASUREMENT

In this analysis, the process

$$e^+e^- \to \gamma\gamma \qquad (2)$$

is used for luminosity measurement. Similar to the process under study (1), the normalizing process (2) does not contain charged particles in the final state. The selection criteria for the process (2) are chosen in such a manner that some uncertainties on the cross section measurement cancel as a result of the normalization.

For example, in the selection of five-photon events of the process under study we require the absence of charged tracks in an event. This leads to loss of signal events that contain beam-generated spurious tracks. The probability of such a loss may reach several percent and strongly depends on experimental conditions (vacuum pressure in the collider beam pipe, beam currents, …). Since the same condition is used for the selection of the normalization process, the systematic uncertainty associated with beam-generated extra tracks cancels. Moreover, events of both processes are selected by the same hardware trigger.

Therefore the uncertainty associated with the trigger inefficiency cancels too.

To select events of the process (2), the following selection criteria are used:

(i) at least two photons and no charged particles are detected,

(ii) the number of hits in the drift chamber is less than or equal to five,

(iii) the energies of the two most energetic photons in an event are larger than $0.3E$,

(iv) the azimuth angles of these photons satisfy the condition $||\phi_1 - \phi_2| - 180°| < 11.5°$,

(v) the polar angles of these photons satisfy the conditions $|\theta_1 + \theta_2 - 180°| < 17.2°$ and $36° < \theta_{1,2} < 144°$.

Photons are reconstructed as clusters in the electromagnetic calorimeter with energies greater than 30 MeV not associated with charged tracks in the drift chamber.

The condition on the number of hits suppresses background from Bhabha events with unreconstructed tracks in the drift chambers. We do not expect any significant background from other e^+e^- annihilation processes in the energy region under study. To estimate possible cosmic-ray background, data recorded during 7.5 hours in a special run without beams are analyzed. No $e^+e^- \to \gamma\gamma$ candidates are selected. We estimate that the fraction of cosmic events in the sample of selected two-photon events is less than 2×10^{-4} and conclude that the cosmic-ray background is negligible.

To calculate the detection efficiency and the cross section of the process (2), a Monte Carlo (MC) event generator based on Ref. [14] is used. The integrated luminosity measured for each energy point is listed in Table I. The theoretical uncertainty on the cross section calculation is about 1%. The systematic uncertainty on the detection efficiency is estimated to be 2%.

IV. EVENT SELECTION

At the first stage of the analysis, five-photon events are selected with the following criteria:

(i) at least five photons and no charged particles are detected,

(ii) the number of hits in the drift chamber is less than or equal to five,

(iii) $E_{tot}/E > 0.5$, where E_{tot} is the total energy deposition in the calorimeter.

For events passing the preliminary selection, kinematic fits to the $e^+e^- \to 5\gamma$ and $e^+e^- \to \pi^0\pi^0\gamma$ hypotheses are performed with requirements of energy and momentum conservation and π^0 mass constraints for the second hypothesis. The goodness of the fits is characterized by the χ^2 parameters: $\chi^2_{5\gamma}$ and $\chi^2_{\pi^0\pi^0\gamma}$. For events with more than five photons, all five-photon combinations are tested and the one with minimal $\chi^2_{\pi^0\pi^0\gamma}$ is used. To select $\omega\pi^0$ candidates, the following additional conditions are applied:

TABLE I. The c.m. energy (E), integrated luminosity (IL), detection efficiency (ε), number of selected signal events (N_s), radiative-correction factor ($1 + \delta$), measured Born cross section (σ). For the cross section the first error is statistical, the second is systematic.

E (GeV)	IL (nb^{-1})	ε (%)	N_s	$1 + \delta$	σ (nb)
1.050	358	35.5	104 ± 11	0.903	$0.90 \pm 0.10 \pm 0.03$
1.075	545	36.5	176 ± 15	0.913	$0.97 \pm 0.08 \pm 0.03$
1.100	845	36.0	297 ± 17	0.921	$1.06 \pm 0.06 \pm 0.04$
1.125	518	35.9	220 ± 16	0.928	$1.28 \pm 0.09 \pm 0.04$
1.150	412	37.8	178 ± 13	0.934	$1.23 \pm 0.09 \pm 0.04$
1.175	539	36.8	231 ± 17	0.939	$1.24 \pm 0.09 \pm 0.04$
1.200	1058	36.6	489 ± 24	0.943	$1.34 \pm 0.06 \pm 0.05$
1.225	550	37.8	265 ± 19	0.947	$1.35 \pm 0.10 \pm 0.05$
1.250	435	37.9	187 ± 17	0.950	$1.19 \pm 0.11 \pm 0.04$
1.275	495	37.0	254 ± 21	0.953	$1.46 \pm 0.12 \pm 0.05$
1.300	1278	37.6	673 ± 35	0.956	$1.47 \pm 0.08 \pm 0.05$
1.325	522	38.2	279 ± 24	0.959	$1.46 \pm 0.12 \pm 0.05$
1.350	554	38.1	292 ± 24	0.962	$1.44 \pm 0.12 \pm 0.05$
1.375	574	38.1	302 ± 24	0.966	$1.43 \pm 0.11 \pm 0.05$
1.400	1012	37.9	578 ± 33	0.970	$1.55 \pm 0.09 \pm 0.05$
1.425	598	38.1	363 ± 26	0.977	$1.63 \pm 0.12 \pm 0.05$
1.450	427	38.3	221 ± 19	0.985	$1.37 \pm 0.12 \pm 0.05$
1.475	599	38.4	291 ± 21	0.995	$1.27 \pm 0.09 \pm 0.04$
1.500	1939	39.0	996 ± 40	1.007	$1.31 \pm 0.05 \pm 0.04$
1.525	487	38.2	245 ± 19	1.021	$1.29 \pm 0.10 \pm 0.05$
1.550	543	38.2	228 ± 16	1.038	$1.06 \pm 0.08 \pm 0.04$
1.575	505	37.9	170 ± 17	1.063	$0.83 \pm 0.08 \pm 0.04$
1.600	814	38.1	232 ± 19	1.100	$0.68 \pm 0.06 \pm 0.03$
1.625	505	37.9	139 ± 15	1.161	$0.63 \pm 0.07^{+0.03}_{-0.04}$
1.650	473	36.9	96 ± 10	1.262	$0.44 \pm 0.04^{+0.02}_{-0.03}$
1.675	454	37.0	74 ± 11	1.429	$0.31 \pm 0.05^{+0.01}_{-0.02}$
1.700	698	30.3	70 ± 10	1.704	$0.19 \pm 0.05^{+0.01}_{-0.01}$
1.725	502	30.6	22 ± 6	2.0–2.3	$0.06 \pm 0.04^{+0.007}_{-0.006}$
1.750	503	29.2	25 ± 6	2.4–3.3	$0.06 \pm 0.04^{+0.02}_{-0.01}$
1.775	521	28.7	22 ± 6	2.8–5.0	$0.03 \pm 0.04^{+0.02}_{-0.01}$
1.800	727	27.9	33 ± 7	3.4–9.0	$0.02 \pm 0.04^{+0.02}_{-0.005}$
1.825	477	28.2	7 ± 3	4–15	$0.004^{+0.027+0.008}_{-0.022-0.0}$
1.850	400	26.7	4^{+4}_{-3}	5–24	$0.002^{+0.037+0.005}_{-0.027-0.0}$
1.870	631	26.2	19 ± 6	5–27	$0.005^{+0.038+0.016}_{-0.033-0.0}$
1.890	577	26.3	24 ± 5	6–31	$0.006^{+0.034+0.022}_{-0.031-0.001}$
1.900	553	24.9	12^{+4}_{-5}	6–40	$0.004^{+0.028+0.011}_{-0.038-0.002}$
1.925	555	24.6	14^{+4}_{-3}	5–68	$0.006^{+0.030+0.013}_{-0.025-0.005}$
1.950	406	23.3	1^{+2}_{-1}	5–63	$0.001^{+0.021+0.001}_{-0.013-0.001}$
1.975	460	24.0	9^{+4}_{-5}	5–39	$0.009^{+0.033+0.008}_{-0.041-0.007}$
2.000	536	23.3	5^{+3}_{-2}	4–39	$0.006^{+0.024+0.005}_{-0.018-0.005}$

(i) $\chi^2_{5\gamma} < 30$ for $E < 1.7$ GeV and $\chi^2_{5\gamma} < 15$ for $E \geq 1.7$ GeV,

(ii) $\chi^2_{\pi^0\pi^0\gamma} - \chi^2_{5\gamma} < 10$,

(iii) at least one of the two $\pi^0\gamma$ invariant masses satisfies the condition $|m_{\pi^0\gamma} - M_\omega| < 200$ MeV/c^2, where M_ω is the ω-meson nominal mass [15].

The distributions of the $\pi^0\gamma$ invariant mass for 7899 selected data events at $E < 1.7$ GeV and 331 data events at $E \geq 1.7$ GeV are shown in Fig. 1. The ω-meson peak is clearly seen in both distributions. Since each event has two entries into the histogram, the nonresonant parts of the distributions are determined mainly by signal events.
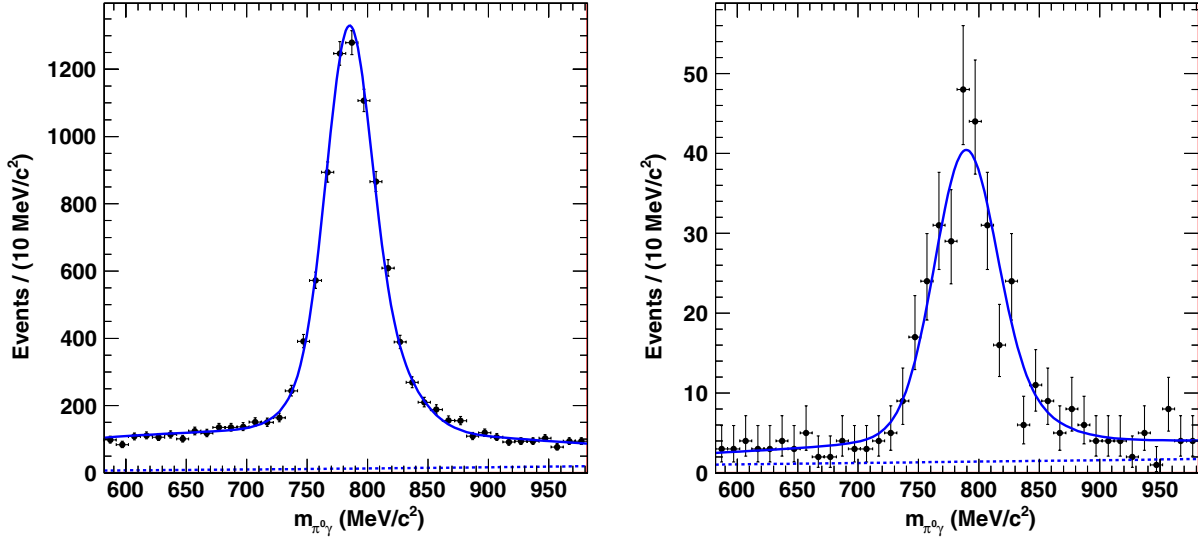
FIG. 1 (color online).   The distribution of the $\pi^0\gamma$ invariant mass for selected data events (points with error bars) with $E < 1.7$ GeV (left) and $E \geq 1.7$ GeV (right). The curves are the result of the fit described in the text. The dashed line represents the linear-background contribution.

V. FITTING THE $\pi^0\gamma$ MASS SPECTRA

To determine the number of signal events, the $\pi^0\gamma$ mass spectrum is fitted by a sum of signal (F_s) and background (F_b) distributions. The signal distribution is obtained by fitting the mass spectrum for simulated signal events with a nonparametric kernel estimation technique [16]. To take into account a difference between data and MC simulation in mass resolution and calibration, the $\pi^0\gamma$ mass for simulated events is smeared and shifted before the fit. The values of the smearing Gaussian sigma (σ_s) and mass shift (Δm) are deduced from comparison of the ω peak width and position in data with the same parameters in simulation. To study energy dependence of σ_s and Δm, a comparison is performed in three c.m. energy regions below 1.7 GeV. The mass shift and the Gaussian sigma are found to be linearly dependent on the energy. The value of Δm changes from (1.0 ± 0.5) MeV/c^2 in the energy region 1.05–1.30 GeV to (3.9 ± 0.5) MeV/c^2 in the energy region 1.5–1.7 GeV. The value of σ_s for the same energy regions changes from (6.2 ± 1.0) MeV/c^2 to (10.5 ± 0.5) MeV/c^2. For energies above 1.7 GeV, where statistics are small, σ_s is obtained by a linear extrapolation from lower energies.

The main sources of background are QED processes such as $e^+e^- \rightarrow 3\gamma$, 4γ, 5γ, and the hadronic processes $e^+e^- \rightarrow \eta\gamma$ and $e^+e^- \rightarrow \omega\pi^0\pi^0$. Background can arise also from the process $e^+e^- \rightarrow \pi^0\pi^0\gamma$ with intermediate states other than the $\omega\pi^0$, for example, $f_2\gamma$. The $\pi^0\gamma$ mass distribution for the QED, $\eta\gamma$ and $\pi^0\pi^0\gamma$ events is expected to be flat and is described by a linear function. The distribution for $\omega\pi^0\pi^0$ events obtained from MC simulation has a complex shape with a wide maximum shifted to the right of the ω peak position. The expected number of $\omega\pi^0\pi^0$ events is calculated using experimental data on

the $e^+e^- \rightarrow \omega\pi^+\pi^-$ cross section [17] and the isotopic relation $\sigma(\omega\pi^+\pi^-) = 2\sigma(\omega\pi^0\pi^0)$. The background from $e^+e^- \rightarrow \omega\pi^0\pi^0$ is important in the energy range 1.7–1.9 GeV, but even there it does not exceed 6% of signal.

The cross section for the process $e^+e^- \rightarrow \rho^0\pi^0 \rightarrow \pi^0\pi^0\gamma$ is estimated from the $e^+e^- \rightarrow \rho\pi \rightarrow 3\pi$ cross section measured by *BABAR* [18], and found to be small, below 1 pb. However, because of closeness of the ρ and ω masses, the interference between the $\omega\pi^0$ and $\rho^0\pi^0$ amplitudes can give a sizable contribution to the measured $e^+e^- \rightarrow \omega\pi^0 \rightarrow \pi^0\pi^0\gamma$ cross section. The $\pi^0\gamma$ spectrum for the interference term is peaked at ω mass and practically indistinguishable from the spectrum for the $\omega\pi^0$ intermediate state. Since the phase between $\omega\pi^0$ and $\rho^0\pi^0$ amplitudes is unknown, we calculate the maximum possible value of the interference term and use this value as an estimate of the systematic uncertainty on the measured $\omega\pi^0$ cross section. The uncertainty due to the interference is estimated to be 2% at $E \leq 1.55$ GeV, then increases to 4.5% at 1.7 GeV and to 8.0% at 1.8 GeV. Above 1.8 GeV this uncertainty is negligible in comparison with the uncertainty of the radiative correction.

To determine the number of signal events we perform an unbinned extended likelihood fit to the mass spectrum in the range $|m_{\pi^0\gamma} - M_\omega| < 200$ MeV/c^2. The likelihood function used for $E < 1.7$ GeV is given as follows:

$$
\begin{aligned}
L = {} & P_P(N; N_s + N_b)P_B(M - N; N, k_t) \\
& \times \prod_{i=1}^{M} \bigg(F_s(m_{\pi^0\gamma}^i) \frac{N_s(1 + k_s)}{N_s(1 + k_s) + N_b(1 + k_b)} \\
& + F_b(m_{\pi^0\gamma}^i) \frac{N_b(1 + k_b)}{N_s(1 + k_s) + N_b(1 + k_b)} \bigg),
\end{aligned} \tag{3}
$$

where N is the number of selected events, M is the total number of entries in the fitted spectrum, N_s (N_b) is the numbers of signal (background) events, and k_s (k_b) is the fraction of signal (background) events with two entries per event, i.e., events for which masses of both $\pi^0\gamma$ combinations satisfy the condition $|m_{\pi^0\gamma} - M_\omega| <$ 200 MeV/c^2, $k_t = (N_s k_s + N_b k_b)/(N_s + N_b)$. The functions P_P and P_B are Poisson and binomial distributions for the total number of selected events and the number of selected events with two entries to the fitted spectrum, respectively. The parameter k_s is calculated using signal MC simulation. It changes from 0.4 at $E = 1.1$ GeV to 0.2 at $E = 2.0$ GeV. To understand the range of k_b variation, we use MC simulation of the $e^+e^- \to \pi^0\pi^0\gamma$ events at the generator level in different models: according to phase space, with the intermediate $f_0(980)\gamma$, $f_2(1270)\gamma$, and $f_0(1370)\gamma$ states. In the energy range under study the k_b value is found to change from 0.1 to 0.5. Therefore, the parameter k_b is set to be 0.3 ± 0.2 in the fit (the likelihood function is multiplied by the corresponding Gaussian). The background distribution F_b is described by a linear function. Above 1.7 GeV a term describing the $\omega\pi^0\pi^0$ contribution is added into the likelihood function.

The fit results are shown in Fig. 1. To obtain the shape of the mass spectrum for the signal, the distribution of simulated events over energy points is weighted to yield the distribution observed in the data. It is seen that our model for signal and background describes well the experimental mass spectra. The total numbers of signal and background events are 7533 ± 110 and 366 ± 70, respectively, for $E < 1.7$ GeV, and 282 ± 22 and 49 ± 15 for $E \geq 1.7$ GeV. A similar fitting procedure is applied in each energy point. The numbers of signal events obtained from the fits are listed in Table I.

VI. DETECTION EFFICIENCY AND RADIATIVE CORRECTIONS

The detection efficiency for the process under study is determined using MC simulation. The simulation includes radiative corrections to the Born cross section calculated according to Ref. [19]. In particular, an extra photon emitted by initial electrons is generated with the angular distribution modeled according to Ref. [20]. The detection efficiency ε_r is evaluated as a function of two parameters: the c.m. energy E and the energy of the extra photon E_r. The E_r dependence of the detection efficiency is shown in Fig. 2 for the energy points with minimum and maximum energies studied.

The visible cross section for the process $e^+e^- \to \omega\pi^0 \to \pi^0\pi^0\gamma$ is written as

$$\sigma_{\rm vis} = \int_0^{x_{\max}} \varepsilon_r(E, xE/2) F(x, E) \sigma(E\sqrt{1 - x}) dx, \quad (4)$$

where $\sigma(E)$ is the Born cross section, which one needs to extract from the experiment; $F(x, E)$ is a function describing the probability to emit extra photons with the total energy $xE/2$ [19]. Equation (4) can be rewritten in the conventional form:

$$\sigma_{\rm vis} = \varepsilon(E)\sigma(E)(1 + \delta(E)), \quad (5)$$

where $\delta(E)$ is the radiative correction, and $\varepsilon(E)$ is defined as follows:

$$\varepsilon(E) \equiv \varepsilon_r(E, 0). \quad (6)$$

Technically the determination of the Born cross section is performed as follows. With the use of Eq. (4) the energy dependence of the measured visible cross section is approximated. To do this the Born cross section is parametrized by some theoretical model that describes data reasonably well. The fitted model parameters are used to evaluate the radiative correction $\delta(E)$. Then the experimental values of the
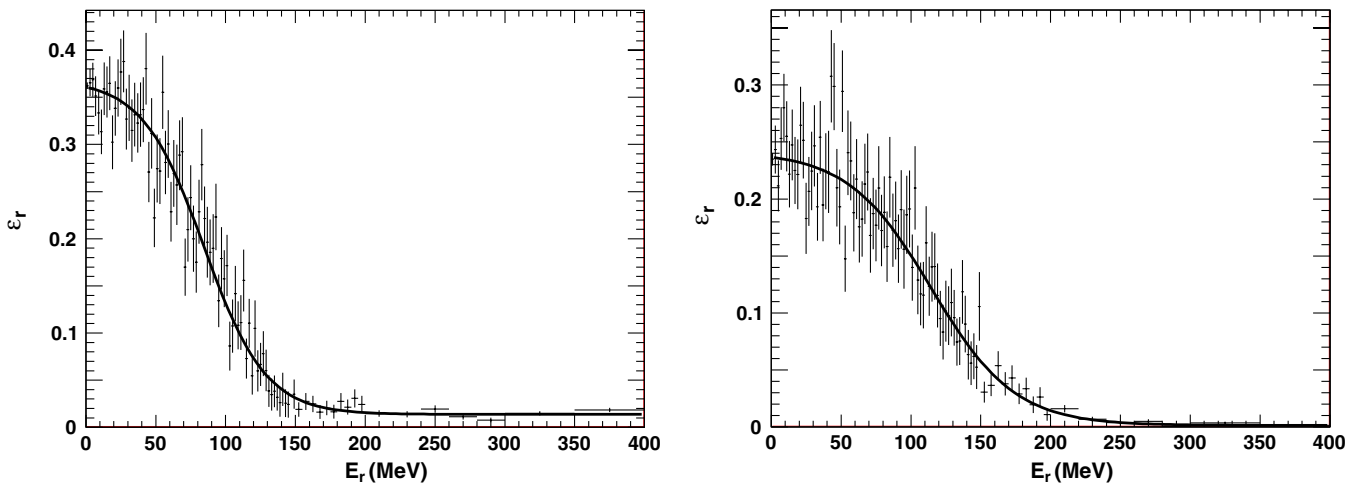

FIG. 2 (color online).   The E_r dependence of the detection efficiency for the process $e^+e^- \to \omega\pi^0 \to \pi^0\pi^0\gamma$ for $E = 1.05$ GeV (left) and $E = 2.00$ GeV (right).
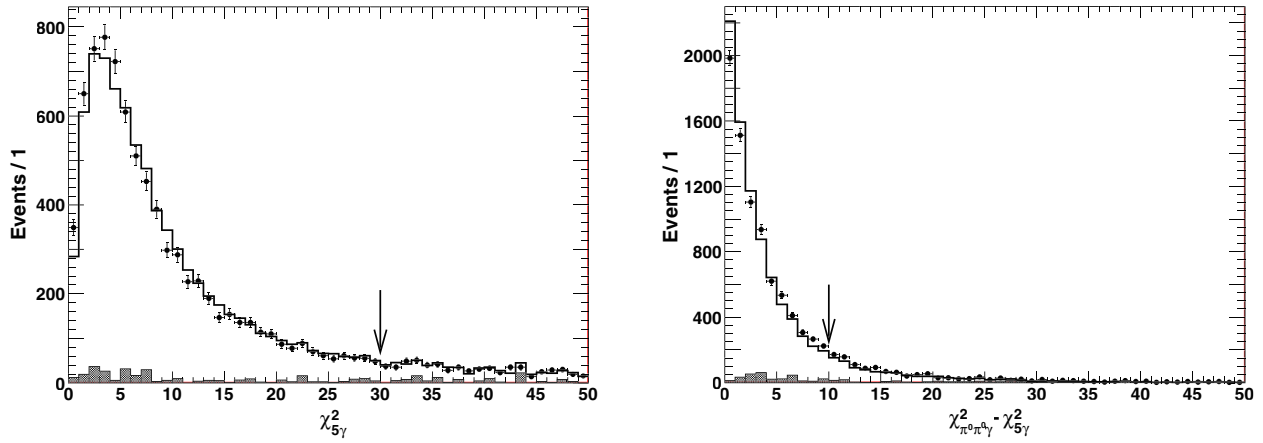
FIG. 3 (color online). The $\chi^2_{5\gamma}$ (left) and $(\chi^2_{\pi^0\pi^0\gamma} - \chi^2_{5\gamma})$ (right) distributions for data events with $E < 1.7$ GeV (points with error bars). The open histogram is a sum of the simulated signal distribution and background distribution. The latter is shown by the shaded histogram. The data and the signal + background distributions are normalized to the same number of events. The arrows indicate the selection criteria used.

Born cross section are obtained using Eq. (5). To estimate the model dependence of the radiative correction, the model parameters are varied in a wide range, with the condition that the approximation quality remains acceptable. The fit to the measured cross section is described in detail in Sec. VII. The obtained values of the radiative correction are listed in Table I. The systematic uncertainty associated with the radiative corrections is estimated to be about 1% at $E < 1.6$ GeV and increases up to 5% at $E = 1.7$ GeV. Above 1.7 GeV the radiative correction becomes large and highly model dependent. For these energy points we quote a range of $(1 + \delta)$ variation.

The imperfect simulation of the detector response for photons leads to a systematic uncertainty in the detection efficiency. To estimate this uncertainty, the data distributions of the most important selection parameters $\chi^2_{5\gamma}$ and $(\chi^2_{\pi^0\pi^0\gamma} - \chi^2_{5\gamma})$ for signal events are compared with corresponding simulated distributions. The distributions are shown in Fig. 3 for events with $E < 1.7$ GeV. They are normalized to the same number of events. The distributions for background events shown in Fig. 3 by the shaded histograms are obtained using data from the $m_{\pi^0\gamma}$ sideband ($66.7 \text{ MeV}/c^2 < |m_{\pi^0\gamma} - M_\omega| < 200.0 \text{ MeV}/c^2$). These background distributions are added to the simulated signal distributions. A difference between the data and MC simulation is seen in both the distributions. To obtain a numerical estimation, we change the limits of the conditions on $\chi^2_{5\gamma}$ and $(\chi^2_{\pi^0\pi^0\gamma} - \chi^2_{5\gamma})$ from 30 to 50 and from 10 to 50, respectively. The resulting variation of the measured cross section $\delta\sigma_{\omega\pi}$ is found to be $(-0.4 \pm 0.5)\%$ for the $\chi^2_{5\gamma}$ condition, and $(2.9 \pm 0.5)\%$ for the $(\chi^2_{\pi^0\pi^0\gamma} - \chi^2_{5\gamma})$ condition. The obtained values of $\delta\sigma_{\omega\pi}$ are used to calculate a correction to the detection efficiency. The detection efficiency obtained from simulation for our standard selection criteria should be decreased by $(-2.5 \pm 0.7)\%$.

In the SND a photon converted in material before the drift chamber produces a track. Events with converted photons are rejected by the selection criteria used. Since the numbers of photons in the final state are different for the signal and normalization processes, the data-MC simulation difference in the conversion probability leads to a systematic shift in the measured cross section. The conversion probability is measured using $\phi \rightarrow \eta\gamma \rightarrow 3\gamma$ events collected in a special run in the vicinity of the ϕ-meson resonance and is found to be $(0.97 \pm 0.28)\%$ in data and $(0.78 \pm 0.04)\%$ in simulation. The data-MC simulation difference $(0.19 \pm 0.28)\%$ is consistent with zero. We conclude that the simulation reproduces the photon conversion reasonably well. The statistical error (0.3%) of the data-MC simulation difference is taken as an estimate of the systematic uncertainty on the photon conversion. The corresponding uncertainty on the measured cross section is estimated as $3 \times 0.3 = 0.9\%$ (the contributions from two of five photons cancel due to normalization).

As it was discussed earlier, some part of the data events contains beam-generated spurious tracks and photons. The effect of extra tracks cancels due to normalization to two-photon events. The presence of extra photons also changes the detection efficiency, but differently for the signal and normalization processes. To take into account this effect in MC simulation, beam-background events recorded during an experiment with a special random trigger are merged with simulated events. The detection efficiencies obtained using simulation with and without merged background are compared. It is found that the presence of extra photons does not influence the number of selected normalization events. The detection efficiency for the signal process increases by 0.3%–1.3% depending on experimental conditions. Unfortunately, the random-trigger events were not recorded on a regular basis during the 2010–2011 experiments. Therefore, we conservatively estimate the correction

due to extra photons to the signal detection efficiency to be 0.8% with a systematic uncertainty of 0.5%.

The corrected values of the detection efficiency $\varepsilon(E)$ are listed in Table I. The statistical error on the detection efficiency is negligible. A systematic uncertainty from the sources discussed above is 1.2%. A nonmonotonic behavior of $\varepsilon(E)$ as a function of the c.m. energy is due to variations of experimental conditions, in particular, due to dead calorimeter channels, a fraction of which changed from 2.4% to 3.4% during the data taking period.

VII. RESULTS AND DISCUSSION

The Born cross section for $e^+e^- \to \omega\pi^0 \to \pi^0\pi^0\gamma$ obtained using Eq. (5) is shown in Fig. 4 in comparison with the results of previous measurements. The numerical values are listed in Table I. The quoted errors on the cross section are statistical and systematic. The sources of systematic uncertainty are summarized in Table II. The total systematic uncertainty is 3.4% in the energy range $E \leq 1.55$ GeV and 4.5% in the energy range $1.55 < E < 1.6$. Above 1.6 GeV the uncertainty increases due to the model dependence of the radiative correction.

Our data are in good agreement with the measurements [5,6] performed by SND and CMD-2 at the VEPP-2M collider at energies below 1.4 GeV, but significantly (by 20%–30%) exceed the DM2 data [10]. The DM2 data were obtained in the $\pi^+\pi^-\pi^0\pi^0$ mode and have been rescaled using the ratio of the $\omega \to \pi^0\gamma$ and $\omega \to 3\pi$ decay probabilities [15].

The cross section measured in this work is fitted together with the SND data obtained in experiments at VEPP-2M [5]. The Born cross section is described by the following formula [5]:
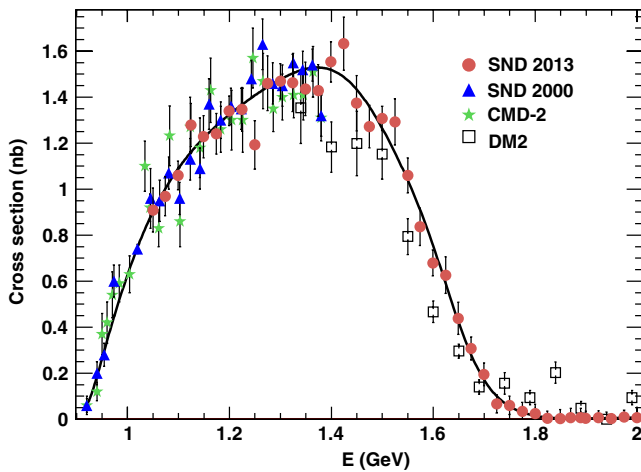

FIG. 4 (color online). The cross section for $e^+e^- \to \omega\pi^0 \to \pi^0\pi^0\gamma$ measured in this work (circles), and in SND [5] (triangles), CMD-2 [6] (stars), and DM2 [10] (squares) experiments. Only statistical errors are shown. The curve is the result of the fit to SND 2000 and SND 2013 data described in the text.

$$\sigma(E) = \frac{4\pi\alpha^2}{E^3}\left(\frac{g_{\rho\omega\pi}}{f_\rho}\right)^2 \left| \frac{m_\rho^2}{D_\rho} + A_1 e^{i\phi_1}\frac{m_{\rho'}^2}{D_{\rho'}} \right.$$
$$\left. + A_2 e^{i\phi_2}\frac{m_{\rho''}^2}{D_{\rho''}} + A_3 \frac{m_{\rho'''}^2}{D_{\rho'''}} \right|^2 P_f(E)B(\omega \to \pi^0\gamma),$$

$$(7)$$

where α is the fine structure constant, $g_{\rho\omega\pi}$ is the $\rho \to \omega\pi$ coupling constant, f_ρ is the $\gamma^* \to \rho$ coupling constant calculated from the $\rho \to e^+e^-$ decay width, $D_{\rho_i}(E) = m_{\rho_i}^2 - E^2 - \iota E\Gamma_{\rho_i}(E)$, m_{ρ_i} and $\Gamma_{\rho_i}(E)$ are the mass and width of the resonance ρ_i, and $B(\omega \to \pi^0\gamma)$ is the $\omega \to \pi^0\gamma$ branching fraction. The first term in Eq. (7) describes the contribution of the $\rho(770)$ resonance, the second and third represent the $\rho(1450)$ and $\rho(1700)$ contributions. The fourth term is added to study a model dependence of the measured cross section due to possible existence of a broad ρ-like resonance with mass $m_{\rho'''} > 2$ GeV/c^2 or due to a nonresonant contribution into the Born cross section near 2 GeV. The parameters A_i are the ratios of the coupling constants $A_i = g_{\rho_i\omega\pi}/g_{\rho\omega\pi} \cdot f_\rho/f_{\rho_i}$; ϕ_1 and ϕ_2 are the phases of the $\rho(1450)$ and $\rho(1700)$ amplitudes relative to the $\rho(770)$ amplitude. For the ρ''' contribution, the phase is assumed to be equal to zero. The energy dependence of the phase-space factor $P_f(E)$ is calculated using the MC event generator for signal events. For an infinitely narrow ω resonance, $P_f(E) = 1/3 \cdot q_\omega^3$, where q_ω is the ω-meson momentum. The energy dependence of the $\rho(770)$ width is described as follows:

$$\Gamma_\rho(E) = \Gamma_\rho(m_\rho)\left(\frac{m_\rho}{E}\right)^2\left(\frac{q_\pi(E)}{q_\pi(m_\rho)}\right)^3 + \frac{g_{\rho\omega\pi}^2}{12\pi}q_\omega^3, \quad (8)$$

where $q_\pi(E) = \sqrt{(E/2)^2 - m_\pi^2}$, and m_π is the π^- mass. For $\rho(1450)$ and $\rho(1700)$, the energy-independent widths are used.

The data are fit with free parameters $g_{\rho\omega\pi}$, A_1, A_2, A_3, $M_{\rho'}$, $M_{\rho''}$, ϕ_1, and ϕ_2. The values of the ρ' and ρ'' widths are fixed at PDG values [15]: $\Gamma_{\rho'} = 400$ MeV and $\Gamma_{\rho''} = 250$ MeV. The parameters $M_{\rho'''}$ and $\Gamma_{\rho'''}$ are set to 2.3 and 400 MeV, respectively. The fit result is shown in Fig. 4. The fitted parameters are used to calculate the values of the radiative corrections listed in Table I. To estimate the model dependence of the radiative correction, the fit is performed with $M_{\rho'}$ fixed at different values from the range 1.4–1.6 GeV and with A_3 either free or fixed at zero. The quality $P(\chi^2; \nu)$ of these fits, where ν is the number of degrees of freedom, varies from 5% to 20%.

To study the contributions of the $\rho(1450)$ and $\rho(1700)$ resonances, we restrict the energy range to $E \leq 1.9$ GeV. This reduces the model uncertainty due to a possible nonresonant contribution or the ρ''' resonance. The parameter A_3 is set to zero. The fit results are presented in Table III. Two models have been studied, with a nonzero and zero ρ''

TABLE II. The systematic uncertainties on the measured cross section from different sources and the correction to the detection efficiency. The total uncertainty is the sum of all the contributions in quadrature.

Source	Systematic uncertainty (%)	Correction (%)
Luminosity	2.2	$\cdots$
Selection criteria	0.7	-2.5
Photon conversion	0.9	$\cdots$
Beam background	0.5	0.8
Radiative correction ($E < 1.6$ GeV)	1	$\cdots$
Interference with $\rho^0 \pi^0$ ($E < 1.6$ GeV)	2–3.6	$\cdots$
Total	3.4–4.5	-1.7

TABLE III. Fit parameters obtained.

Parameter	Model 1	Model 2
$g_{\rho\omega\pi}$, GeV^{-1}	15.6 ± 0.3	17.4 ± 0.1
A_1	0.26 ± 0.01	0.11 ± 0.001
A_2	0.060 ± 0.006	$\equiv 0$
$M_{\rho'}$, MeV	1491 ± 19	1488 ± 3
$\Gamma_{\rho'}$, MeV	$\equiv 400$	321 ± 4
$M_{\rho''}$, MeV	1708 ± 41	$\cdots$
$\Gamma_{\rho''}$, MeV	$\equiv 250$	$\cdots$
ϕ_1, deg	168 ± 3	121 ± 2
ϕ_2, deg	10 ± 7	$\cdots$
χ^2/ν	$56.8/52$	$118.6/54$

contribution. In the fit with the second model the parameter $\Gamma_{\rho'}$ is left free. Such a fit with only one ρ excitation was performed in Ref. [6] and gave a reasonable description of CMD-2 and DM2 data. It is seen that our more precise data cannot be described by the model with one excited ρ state. The fitted value of the parameter A_i is used to calculate the products of the branching fractions

$$B(\rho_i \to \omega\pi^0) \cdot B(\rho_i \to e^+e^-) = \frac{\sigma_{\rho_i}(m_{\rho_i})m_{\rho_i}^2}{12\pi}, \quad (9)$$

where

$$\sigma_{\rho_i}(E) = \frac{4\pi\alpha^2}{E^3}\left(\frac{g_{\rho\omega\pi}}{f_\rho}\right)^2 \left| A_i \frac{m_{\rho_i}^2}{D_{\rho_i}} \right|^2 P_f(E) \quad (10)$$

is the cross section for the process $e^+e^- \to \rho_i \to \omega\pi^0$ without interference with other ρ-like resonances. The results are following

$$B(\rho' \to e^+e^-) \cdot B(\rho' \to \omega\pi^0) = (5.3 \pm 0.4) \times 10^{-6},$$

$$B(\rho'' \to e^+e^-) \cdot B(\rho'' \to \omega\pi^0) = (1.7 \pm 0.4) \times 10^{-6}.$$

$$(11)$$

It should be noted that at the moment there is no generally accepted approach for describing the tail of the $\rho(770)$ resonance above 1 GeV and shapes of broad resonances like ρ' and ρ''. The excitation curves of the three resonances

ρ, ρ', and ρ'' overlap; their amplitudes strongly interfere with each other. As a result, a small change of the resonance shape can lead to significant shifts in fitted resonance parameters. So, the results obtained with our very simple model using energy-independent ρ' and ρ'' widths can be considered only as rough estimates of the resonance parameters.

The cross section for $e^+e^- \to \omega\pi^0$ can be expressed in terms of the $\gamma^* \to \omega\pi^0$ transition form factor $F_{\omega\pi\gamma}(q^2)$ [21,22], where q is the four-momentum of the virtual photon:

$$\sigma_{\omega\pi^0}(E) = \frac{4\pi\alpha^2}{E^3}|F_{\omega\pi\gamma}(E^2)|^2 P_f(E). \quad (12)$$

This form factor is also measured in the $\omega \to \pi^0 e^+e^-$ [23,24] and $\omega \to \pi^0 \mu^+\mu^-$ [25,26] decays. The value of the form factor at $q^2 = 0$ is related to the $\omega \to \pi^0\gamma$ partial width:

$$\Gamma(\omega \to \pi^0\gamma) = \frac{\alpha}{3}P_\gamma^3|F_{\omega\pi\gamma}(0)|^2, \quad (13)$$

where P_γ is the decay photon momentum. Using Eqs. (7), (12), and (13), and data from Table III, we calculate $\Gamma(\omega \to \pi^0\gamma)$ for model 1 to be 0.88 ± 0.05 MeV. For such a simple model the agreement with the experimental value $\Gamma(\omega \to \pi^0\gamma) = 0.703 \pm 0.024$ MeV [15] looks reasonable.

Figure 5 shows the normalized transition form factor squared ($|F_{\omega\pi\gamma}(q^2)/F_{\omega\pi\gamma}(0)|^2$) measured in this work and in Ref. [5] together with most precise data from omega decays obtained in the NA60 experiment [26]. The curve represents the results of the model prediction with the parameters listed in Table III for model 1. The dashed curve shows the $\rho(770)$ contribution. We conclude that it is hard to describe data from e^+e^- annihilation and the $\omega \to \pi^0\mu^+\mu^-$ decay simultaneously with our model based on vector meson dominance.

The CVC hypothesis establishes a relation between the charged hadronic current in the τ decay and the isovector part of the electromagnetic current. So, the $e^+e^- \to \omega\pi^0$ cross section can be related with the spectral function of the $\tau^- \to \omega\pi^-\nu_\tau$ decay ($V_{\omega\pi}$) [3]:
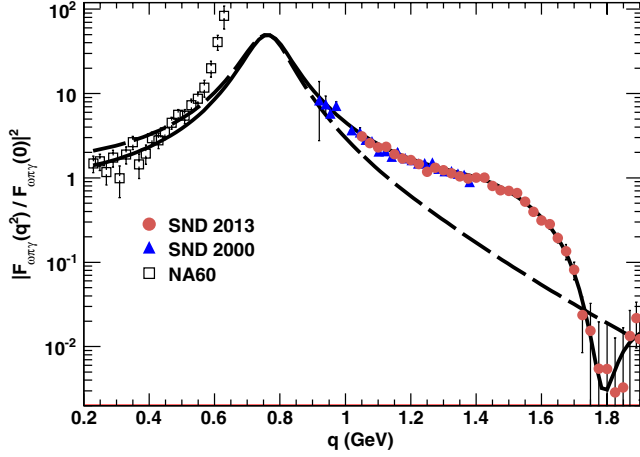
FIG. 5 (color online). The $\gamma^* \to \omega\pi^0$ transition form factor. The points with error bars represent data from this work (circles), Ref. [5] (triangles), and Ref. [26] (squares). Only statistical errors are shown. The curve represent the result of model prediction with the parameters listed in Table III for model 1. The dashed curve shows the $\rho(770)$ contribution.

$$\sigma_{\omega\pi^0}(E) = \frac{4\pi^2\alpha^2}{E^2} V_{\omega\pi}(E). \tag{14}$$

The comparison of the $e^+e^- \to \omega\pi^0 \to \pi^0\pi^0\gamma$ cross section measured by SND with the cross section calculated under the CVC hypothesis from the $\tau^- \to \omega\pi^- \nu_\tau$ spectral function measured in the CLEO experiment [27] is presented in Fig. 6. It is seen that the e^+e^- and τ data are in reasonable agreement. The χ^2/ν (ν is the number of degrees of freedom) of the comparison between the CLEO data and our fitted curve is 19.7/16. To calculate
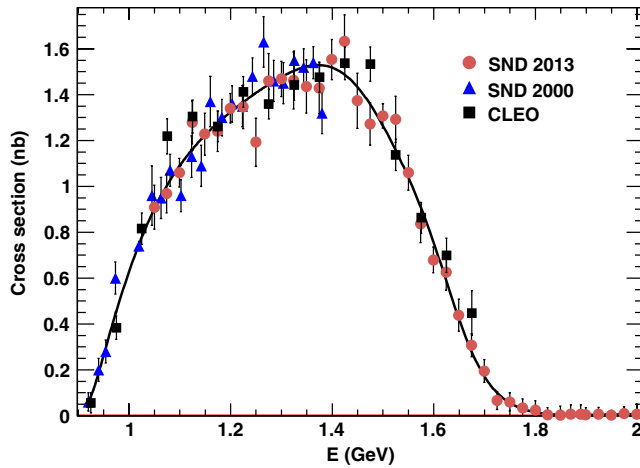

FIG. 6 (color online). The cross section for $e^+e^- \to \omega\pi^0 \to \pi^0\pi^0\gamma$ measured in this work (circles) and in Ref. [5] (triangles). Only statistical errors are shown. The cross-section data shown by squares was calculated under the CVC hypothesis from the spectral function of the $\tau \to \omega\pi\nu_\tau$ decay measured in the CLEO experiment [27]. The curve is the result of the fit to SND 2013 and SND 2000 data.

this χ^2, a 5% systematic uncertainty of CLEO data [27] was taken into account.

A more quantitative test of the CVC hypothesis can be made by comparing the measured $\tau \to \omega\pi\nu_\tau$ branching fraction with the value calculated from the $e^+e^- \to \omega\pi^0$ cross section according to the formula [3,27]

$$\Gamma(\tau^- \to \omega\pi^- \nu_\tau)$$
$$= \frac{G_F^2|V_{ud}|^2}{64\pi^4\alpha^2 m_\tau^3} \int^{m_\tau} q^3(m_\tau^2 - q^2)^2(m_\tau^2 + 2q^2)\sigma_{\omega\pi^0}(q)dq, \tag{15}$$

where $|V_{ud}|$ is the Cabibbo-Kobayashi-Maskawa matrix element, m_τ is the τ lepton mass, and G_F is the Fermi constant. We integrate the fitted curve shown in Fig. 4 and obtain the value of the product $\Gamma(\tau^- \to \omega\pi^- \nu_\tau)B(\omega \to \pi^0\gamma) = (3.68 \pm 0.04 \pm 0.13) \times 10^{-6}$ eV. Using the values of the τ lifetime and $B(\omega \to \pi^0\gamma)$ we calculate the branching fraction

$$B(\tau^- \to \omega\pi^- \nu_\tau) = (1.96 \pm 0.02 \pm 0.10) \times 10^{-2}, \tag{16}$$

which is in good agreement with the experimental value $(1.95 \pm 0.08) \times 10^{-2}$ obtained as a difference of the PDG [15] values for $B(\tau^- \to \omega h^- \nu_\tau)$ and $B(\tau^- \to \omega K^- \nu_\tau)$. We conclude that the CVC hypothesis for the $\omega\pi$ system works well within the reached experimental accuracy of about 5%.

VII. SUMMARY

The cross section for the $e^+e^- \to \omega\pi^0 \to \pi^0\pi^0\gamma$ process has been measured with the SND detector at the VEPP-2000 e^+e^- collider in the energy range of 1.05–2.00 GeV. This is the most accurate measurement of the $e^+e^- \to \omega\pi^0$ cross section between 1.4 and 2.0 GeV. Below 1.4 GeV our data agree with the earlier measurements of the same reaction performed at the VEPP-2M collider with the SND [5] and CMD-2 [6] detectors. Significant disagreement is observed with DM2 data [10] in the energy range 1.3–2.0 GeV.

Data on the $e^+e^- \to \omega\pi^0$ cross section are well described by the vector meson dominance model with the three ρ-like state: $\rho(770)$, ρ', and ρ''. However, the full data set on the $\gamma^* \to \omega\pi^0$ transition form factor including data from both e^+e^- annihilation and ω decays, in particular, $\omega \to \pi^0\mu^+\mu^-$ [26], cannot be described by such a simple model.

We have also tested the CVC hypothesis comparing the energy dependence of the $e^+e^- \to \omega\pi^0$ cross section with the spectral function for the $\tau^- \to \omega\pi^- \nu_\tau$ decay, and calculating the branching fraction for this decay from e^+e^- data. We have concluded that the CVC hypothesis for the $\omega\pi$ system works well within the experimental accuracy of 5%.

ACKNOWLEDGMENTS

[1] M. N. Achasov *et al.*, Nucl. Instrum. Methods Phys. Res., Sect. A **598**, 31 (2009); V. M. Aulchenko *et al.*, *ibid.* **598**, 102 (2009); A. Yu. Barnyakov *et al.*, *ibid.* **598**, 163 (2009); V. M. Aulchenko *et al.*, *ibid.* **598**, 340 (2009).

[2] Yu. M. Shatunov *et al.*, in *Proceedings of the 7th European Particle Accelerator Conference, Vienna, 2000*, p. 439, http://accelconf.web.cern.ch/AccelConf/e00/PAPERS/MOP4A08.pdf.

[3] Y.-S. Tsai, Phys. Rev. D **4**, 2821 (1971); **13**, 771(E) (1976).

[4] S. I. Dolinsky *et al.*, Phys. Lett. B **174**, 453 (1986).

[5] M. N. Achasov *et al.* (SND Collaboration), Phys. Lett. B **486**, 29 (2000).

[6] R. R. Akhmetshin *et al.* (CMD-2 Collaboration), Phys. Lett. B **562**, 173 (2003).

[7] V. M. Aulchenko *et al.* (SND Collaboration), Zh. Eksp. Teor. Fiz. **117**, 1067 (2000) [J. Exp. Theor. Phys. **90**, 927 (2000)].

[8] F. Ambrosino *et al.* (KLOE Collaboration), Phys. Lett. B **669**, 223 (2008).

[9] M. N. Achasov *et al.* (SND Collaboration), JETP Lett. **94**, 734 (2012).

[10] D. Bisello *et al.*, Nucl. Phys. B, Proc. Suppl. **21**, 111 (1991).

[11] M. N. Achasov *et al.* (SND Collaboration), J. Exp. Theor. Phys. **96**, 789 (2003).

[12] R. R. Akhmetshin *et al.* (CMD-2 Collaboration) Phys. Lett. B **466**, 392 (1999).

[13] E. V. Abakumova, M. N. Achasov, D. E. Berkaev, V. V. Kaminsky, N. Yu. Muchnoi, E. A. Perevedentsev, E. E. Pyata, and Yu. M. Shatunov, Phys. Rev. Lett. **110**, 140402 (2013).

[14] F. A. Berends and R. Kleiss, Nucl. Phys. **B186**, 22 (1981).

[15] J. Beringer *et al.* (Particle Data Group), Phys. Rev. D **86**, 010001 (2012).

[16] K. S. Cranmer, Comput. Phys. Commun. **136**, 198 (2001).

[17] B. Aubert *et al.* (BABAR Collaboration), Phys. Rev. D **76**, 092005 (2007); **77**, 119902(E) (2008).

[18] B. Aubert *et al.* (BABAR Collaboration), Phys. Rev. D **70**, 072004 (2004).

[19] E. A. Kuraev and V. S. Fadin, Yad. Fiz. **41**, 733 (1985) [Sov. J. Nucl. Phys. **41**, 466 (1985)].

[20] G. Bonneau and F. Martin, Nucl. Phys. **B27**, 381 (1971).

[21] L. G. Landsberg, Phys. Rep. **128**, 301 (1985).

[22] S. Pacetti, Eur. Phys. J. A **38**, 331 (2008).

[23] R. R. Akhmetshin *et al.* (CMD-2 Collaboration), Phys. Lett. B **613**, 29 (2005).

[24] M. N. Achasov *et al.* (SND Collaboration), JETP **107**, 61 (2008).

[25] R. I. Dzhelyadin *et al.* Phys. Lett. **102B**, 296 (1981); JETP Lett. **33**, 228 (1981).

[26] R. Arnaldi *et al.* (NA60 Collaboration), Phys. Lett. B **677**, 260 (2009).

[27] K. W. Edwards *et al.* (CLEO Collaboration), Phys. Rev. D **61**, 072003 (2000).